Steel and Composite Structures, *Vol. 31*, *No. 4* (*2019*) *329-340*
DOI: https://doi.org/10.12989/scs.2019.31.4.329

Investigation on mechanical performance of flat steel plate-lightweight aggregate concrete hollow composite slab

Yong Yang, Yang Chen*, Ye Yang and Susheng Zeng

School of Civil Engineering, *Xi'an University of Architecture & Technology*, *Xi'an*, *Shaanxi 710055*, *China*

(*Received March 15*, *2018*, *Revised February 28*, *2019*, *Accepted April 28*, *2019*)

Abstract. An innovated type of the flat steel plate-lightweight aggregate concrete hollow composite slab was presented in this paper. This kind of the slab is composed of flat steel plate and the lightweight aggregate concrete slab, which were interfaced with a set of perfobond shear connectors (PBL shear connectors) with circular hollow structural sections (CHSS) and the shear stud connectors. Five specimens were tested under static monotonic loading. In the test, the influence of shear span/height ratios and arrangements of CHSS on bending capacity and flexural rigidity of the composite slabs were investigated. Based on the test results, the crack patterns, failure modes, the bending moment-curvature curves as well as the strains of the flat steel plate and the concrete were focused and analyzed. The test results showed that the flat steel plate was fully connected to the lightweight aggregate concrete slab and no obvious slippage was observed between the steel plate and the concrete, and the composite slabs performed well in terms of bending capacity, flexural rigidity and ductility. It was further shown that all of the specimens failed in bending failure mode regardless of the shear span/height ratios and the arrangement of CHSS. Moreover, the plane-section assumption was proved to be valid, and the calculated formulas for predicting the bending capacity and the flexural rigidity of the composite slabs were proposed on the basis of the experimental results.

Keywords: steel plate-concrete hollow composite slab; mechanical behavior; bending capacity; flexural rigidity; static test

1. Introduction

In recent years, steel-concrete composite slabs have been widely used in the industrial and civil construction due to their considerable advantages such as omitting formwork and scaffolding and continuous high-quality and high-speed construction (Altoubat *et al*. 2015, Kataoka *et al*. 2017, Mirza *et al*. 2016, Qiao *et al*. 2015, Siekierski 2016, Yang *et al*. 2016). A good example is the composite slabs with profiled steel sheet, which have been extensively studied around the world for many years (Al-Deen *et al*. 2011, Ferrer *et al*. 2018, Jiang *et al*. 2018, Johnson 2008, Leon *et al*. 2006, Oehlers and Bradford 1995, Uy and Bradford 1996). However, the thickness of the profiled steel sheet is generally in the range of 0.75 mm to 2.5 mm, which results in the steel-concrete composite slabs with profiled steel sheet would not be applied in the large span floors slabs or bridge decks without the temporary scaffolding or secondary beam to sustaining the construction load. If the secondary beams and the temporary scaffoldings are adopted in engineering, the net height of the floor would be reduced, and the labor cost and the construction time would be increased significantly. Most importantly, with the increase of the structural span, it is of crucial importance to decrease the deadweight of the superstructure. Therefore, the normal concrete is not suitably applied to high-rise and long-span buildings because of its larger apparent density and inferior seismic performance.

To solve the problem of the composite slabs with steel profiled sheet, the flat steel plate-lightweight aggregate concrete hollow composite slabs are proposed and introduced. As presented in Fig. 1, this type of the composite slab is composed of the bottom flat steel plate, lightweight aggregate concrete slab and perfobond rib connectors (PBL connectors). It is relatively easy to fabricate this hollow composite slab. Firstly, welding the PBL plate with a set of the holes to the bottom flat steel plate, and then inserting the steel pipes into the circular holes of the PBL plate and welding them seamlessly, finally pouring the lightweight aggregate concrete. For such type of composite slab, it is convenient to fabricate the flat steel plate because neither the complex construction procedure nor the special moulding machine is necessary. Furthermore, the thickness of the flat steel plate can be utilized as expected and the CHSS inserted in the hole of the PBL plate can effectively reduce the self weight of the composite slab and improve the bending capacity and the stiffness of the slabs. Additionally, the lightweight aggregate concrete was adopted owing to its advantages such as lower weight, good fire resistance, lower thermal conductivity and better durability (Ekmekyapar *et al*. 2017, Tang 2017, Zhang *et al*. 2012). Therefore, the span of the floor slab or the bridge deck could be as larger as needed, no secondary beam and temporary scaffolding are required and consequently the engineering cost and the labor time of the composite slabs are greatly saved.

*Corresponding author, Ph.D. Candidate,
E-mail: xauatchenyang@126.com

http://www.techno-press.org/?journal=scs&subpage=6
ISSN: 1229-9367 (Print), 1598-6233 (Online)

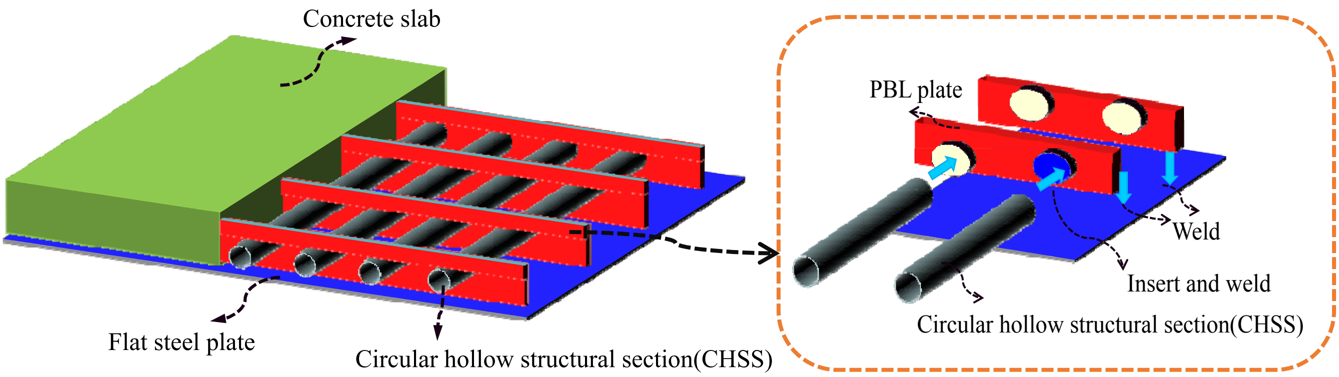

Fig. 1 Diagram of the composite slab

In this type of the composite slab, the flat steel plates are fully bonded to the concrete by the PBL shear connectors and the shear studs welded on the surface of the flat steel plate. Here, the bottom flat steel plate can be regarded as the longitudinal reinforced bars and the formwork, and there is no reinforcement required, which result in a great deal of saving in steel cost and labor time. Meanwhile, many studies have been conducted involving push-out tests and numerical simulations to investigate the behavior of PBL connectors (Ahn *et al.* 2010, Al-Darzi *et al.* 2007, Oguejiofor and Hosain 1994, Su *et al.* 2016, Vianna *et al.* 2013, Wei *et al.* 2015, Zheng *et al.* 2016). In this study, the PBL shear connector is composed of PBL plate, concrete in the hole and steel pipes passed through the hole, which are not only used to resist the shear force between the steel and the concrete but also improve the bending capacity and the bending rigidity of the slab during the construction. Therefore, the innovated composite slab proposed in this study shows a great deal of advantages such as light weight, high bending capacity, high flexural rigidity, superior seismic behavior, and cost-saving in special moulding machine and temporary scaffolding as well as convenient construction for large-span building floors or bridge decks.

To investigate the mechanical performance of such composite slab, an experimental program with five specimens were conducted. In this paper, the parameters including the shear span/height ratios and the arrangement of the CHSS were focused and investigated. Moreover, the crack patterns and failure modes as well as the strains of the steel plate and the concrete were examined. Based on the experimental results, corresponding formulas for calculating the bending capacity and flexural rigidity of the composite slab were put forward and presented.

2. Experimental study

2.1 Specimens

A total of five flat steel plate-lightweight aggregate concrete hollow composite slab specimens were tested to failure under static loading. In this test, the specimens were divided into two series. For these two series specimens, the spans and the cross sections were almost identical. The span, width and height of all five specimens were 2400 mm, 620 mm and 200 mm, respectively. The difference of the specimens in series 1 and series 2 is the arrangement of the CHSS passed through the holes at the PBL shear connectors, which is aiming to investigate the influence of the different arrangement of the CHSS on the mechanical performance of the composite slabs at the orthogonal directions. In series 1, the steel tubes were arranged at the longitudinal direction of the slabs and spaced at the interval of 65 mm, and the shear span/height ratios of the specimens were 3.85 and 2.00 as well as the shear span lengths were 770 mm and 400 mm for specimen HCS1 and HCS2, respectively. In series 2, the steel tubes were arranged at the transverse direction of the slabs with an interval of 65 mm, but the shear span/height ratios were 3.85, 4.50 and 5.00 for specimens HCS3, HCS4 and HCS5 respectively.

In all the specimens, the steel tubes were placed at the holes of the PBL shear connectors to resist the longitudinal shear force and vertical uplift force on the interface of steel plate and concrete, the external diameter and wall thickness of the steel tube were 125 mm and 3 mm, respectively. Furthermore, to achieve good composite action between flat steel plate and concrete, the stud shear connectors with the size of the 16 mm diameter and 65 mm height were welded

Table 1 Details of the hollow composite decks specimens

Series No.	Specimen No.	Span l_0 (mm)	Width b (mm)	Height h (mm)	Shear span a (mm)	Shear span/height ratio λ	Arrangement of the steel pipes
1	HCS1	2400	620	200	770	3.85	In the Longitudinal direction
	HCS2	2400	620	200	400	2.00	In the Longitudinal direction
2	HCS3	2400	620	200	770	3.85	In the transverse direction
	HCS4	2400	620	200	900	4.50	In the transverse direction
	HCS5	2400	620	200	1000	5.00	In the transverse direction

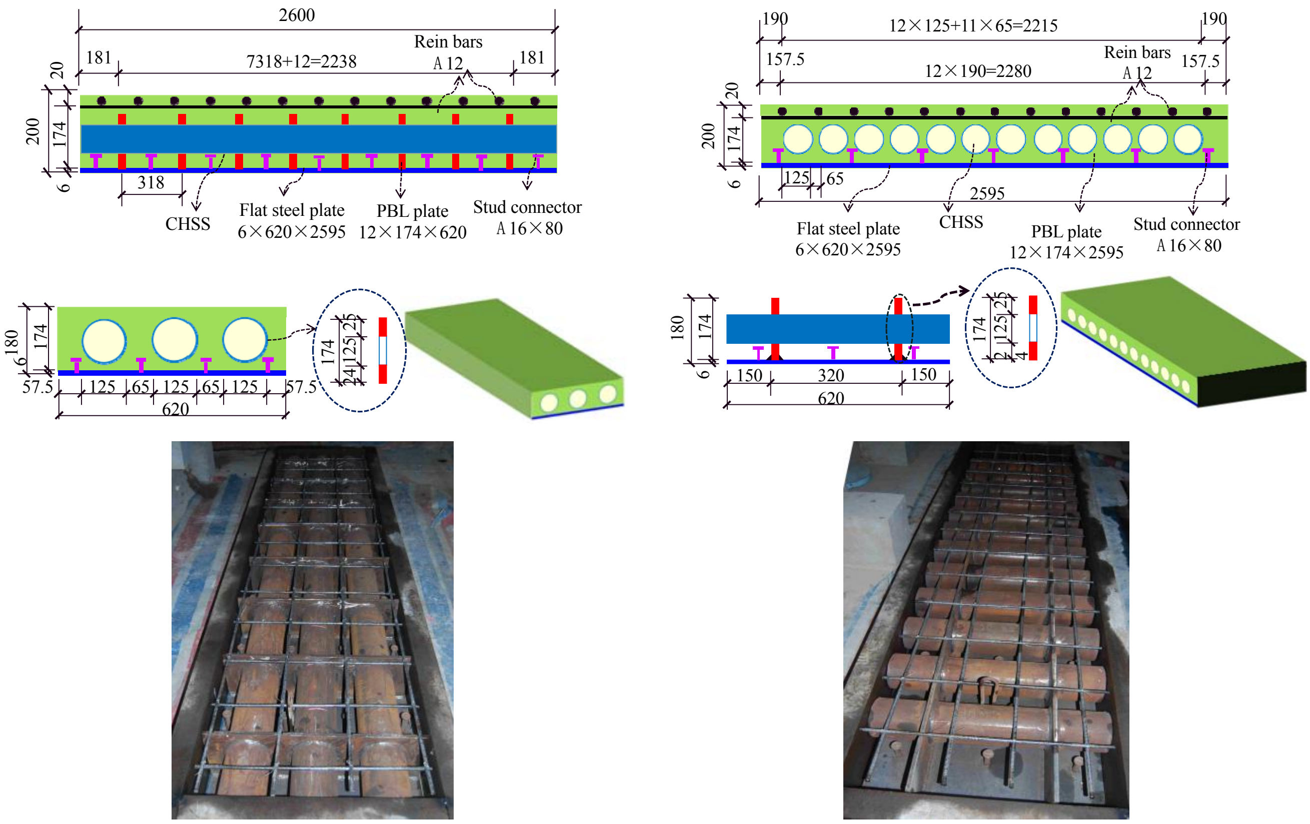

(a) Schematic of the specimen in series 1 (b) Schematic of the specimen in series 2

Fig. 2 Section details of the hollow composite slab specimens

Table 2 Measured material properties

Material	Thickness/Diameter (mm)	Yielding strength f_y (MPa)	Ultimate strength f_u (MPa)	Elastic Modulus E (MPa)
Steel plate	6	300	410	2.05×10^5
PBL plate	12	331	518	2.05×10^5
Reinforcing steel bar	12	320	425	2.10×10^5
CHSS	3	284	407	2.10×10^5

at the surface of the flat steel plate, but the influence of the stud shear connectors on the mechanical behavior of the hollow composite slab was not considered in this study. Details of the specimens are summarized in Table 1 and the cross section of the composite slab specimens is depicted in Fig. 2.

2.2 Material properties

In both series of specimens, the thicknesses of the flat steel plate and the PBL plate were 6 mm and 12 mm, respectively. A12 bars of 12 mm in diameter and HPB235 in grade were used as the reinforcing steel bars. The detailed properties listed in Table 2 were determined by the tensile tests samples taken from the flat steel plate, the PBL plate and the reinforcing bars according to Chinese steel standard (GB/T 700-2006). The strength grades of the lightweight aggregate concrete in composite slabs were identical and were designed as C40, the average value of the cubic compressive strength and the prismatic compressive strength are 39.0 MPa and 27.21 MPa, as well as Young’s modulus is16.0 GPa.

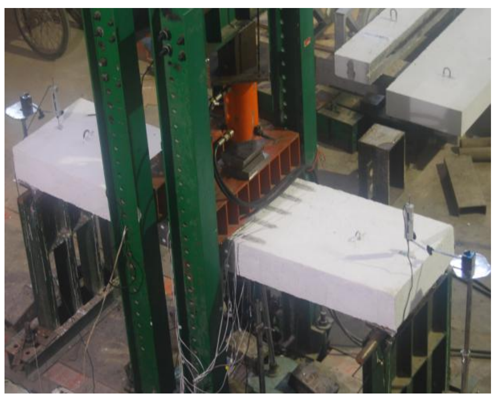

Fig. 3 Photo of the test setup

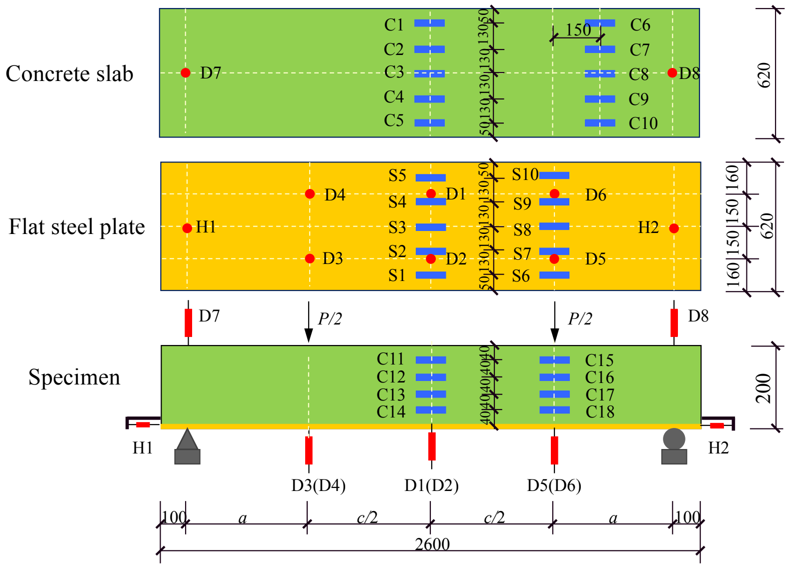

Fig. 4 Layout of the LVDTs and strain gauges

Specimen HCS1

Specimen HCS2

(a) The failure mode of the specimens in series 1

Specimen HCS4

Specimen HCS5

(b)The failure mode of the specimens in series 2

Fig. 5 The typical failure modes of the specimens

2.3 Test setup and instrument

Both series of composite slab specimens were conducted on a 2000 kN capacity hydraulic testing machine. A four-point symmetrical loading method was adopted and the load was applied on the specimens in a monotonic manner as presented in Fig. 3. During the test, linear variable displace-ent transducers (LVDTs) were used to record the deflections of the mid span point, the loading point and two supports. A set of strain gauges were used to measure the strain responses of the concrete and the flat steel plate. In addition, two horizontal LVDTs were installed on both ends of the specimens to monitor the slip of the steel plate and the concrete slab. The details of the layout of LVDTs and the strain gauges in specimens are plotted in Fig. 4.

3. Test results and discussions

3.1 Failure modes

Fig. 5(a) illustrates the failure modes of the specimens in series 1. Two specimens in series 1 failed in typical bending failure, with the yielding of the bottom flat steel plate and the crushing of the concrete in the compression region. For specimen HCS1, when the load was up to about 110 kN, the initial flexural cracks occurred in pure bending section at the mid-span of the specimen, and these cracks fully developed and no inclined cracks were observed in shear span region until the failure of the specimen. For specimen HCS2, when the load was up to 184 kN, the inclined cracks headed to the loading point appeared in the shear span, and then the micro flexural cracks occurred at the pure bending section. With the loading increasing, the inclined cracks and the flexural cracks propagated quickly in quantity and width. When the specimen HCS2 was loaded about 280 kN, main flexural crack was formed and stretched to the top of the slab but the development of the inclined crack was not notable. With the further increasing of the load, the top concrete crushing in the compression region at the pure bending section was observed, with the mid-span deflection increasing quickly and the load dropping suddenly.

Fig. 5(b) shows the failure modes of the specimens in series 2. The failure mode of the specimen HCS3 was similar to that of the specimen HCS4 regardless of the shear span/height ratios. Therefore, only the cracks development progress of the specimen HCS4 is described. When the load was up to approximately 57 kN, the inclined crack between two steel pipes appeared in the shear span region of the specimen. As the load increasing, several fine inclined cracks initiated from the upper surface of the steel pipes and extended to the loading point. When the load was increased to the ultimate load P_u, a longitudinal crack at the interface between the concrete slab and the steel pipes was formed because of their poor bond performance. Moreover, the top concrete at the compression region was crushed, which demonstrated the final failure mode of specimen HCS4 was close to the bending failure of oblique cross section. For specimen HCS5, which failed in typical bending failure mode similar to that of the specimen HCS1. It is noted that some effective measures should be taken to avoid the oblique cross section bending failure mode of the hollow composite slab with transverse steel pipes in practical engineering.

3.2 Bending moment - curvature curves

The main experimental results are tabulated in Table 3, and the bending moment-curvature curves at the mid-span of each hollow composite specimen are plotted in Fig. 6. From the bending moment-curvature curves, it can be seen the bending capacity of specimen HCS1 is higher than that of specimen HCS2, due most likely to the coupling effect of bending and shear in specimen HCS2. It also can be observed from the curves that the bending capacity of specimen HCS5 is similar to that of the specimen HCS3 and HCS4, but the specimen HCS3 and HCS4 failed in bending failure of oblique cross section have a smaller ductility than the specimen HCS5 failed in typical bending. As far as stiffness is concerned, all of specimens present approximately the same stiffness up to their maximum bending moment, which means that the hollow composite slabs proposed in this paper have almost the same stiffness in orthogonal directions.

From the bending moment-curvature curves, the ductility ratios of the slabs except that of the specimen HCS2 are calculated as listed in Table 3. The ductility ratio is determined as the value of the ultimate mid-span deflection Δ_u divides by the yielding mid-span deflection Δ_y, which is defined as the corresponding deflection of the specimen subjected to the yielding moment M_y. The yielding moment M_y is determined from the yielding shear force $P_y/2$ multiplies by the shear span length a of each specimen. Here, P_y and M_y represent the measured values of the load and the bending moment when the bottom steel plate yields. P_u and M_u represent the ultimate load and the ultimate bending moment of the specimens. The ductility ratio of the specimen HCS2 is not obtained due to the absence of the strain of the bottom steel plate during the experiment. It is apparent from Fig. 6 that good ductile behavior for both series of the specimens is observed during the test, but the deformability of the composite slabs with longitudinal CHSS is slightly better than that of the slabs with transverse CHSS.

3.3 Validation of the plane section assumption

The curves of the ultimate load versus the strains of the concrete in compression zone and the bottom steel plate for

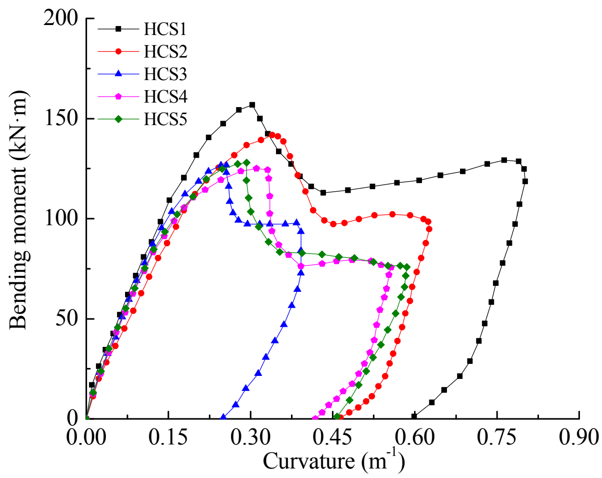

Fig. 6 Bending moment vs. curvature curves at the middle span point of the specimens

Table 3 Main test results of the specimens

Series No.	Specimen No.	P_y (kN)	M_y (kN·m)	P_u (kN)	M_u (kN·m)	M_{cu} (kN·m)	Δ_y (mm)	Δ_u (mm)	$\mu = \Delta_u / \Delta_y$
1	HCS1	130	50.05	406	156.3	134.25	6.2	30.0	4.84
	HCS2	/	/	703	140.6	134.25	/	/	/
2	HCS3	292	88	330	127.05	114.8	12.8	25.4	1.98
	HCS4	195	87.5	278	125.1	114.8	13.6	32.5	2.39
	HCS5	150	75	254	127	114.8	10.0	28.4	2.84

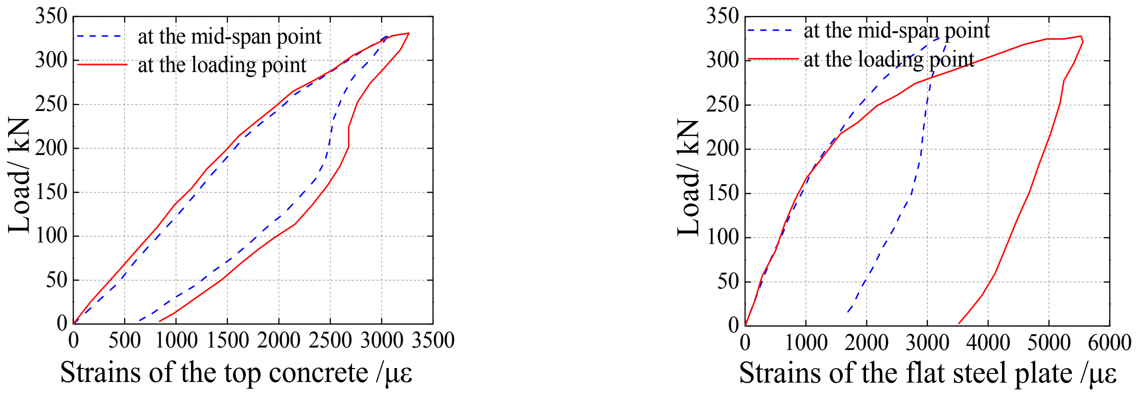

Fig. 7 Load vs. strains curves of the specimen HCS3

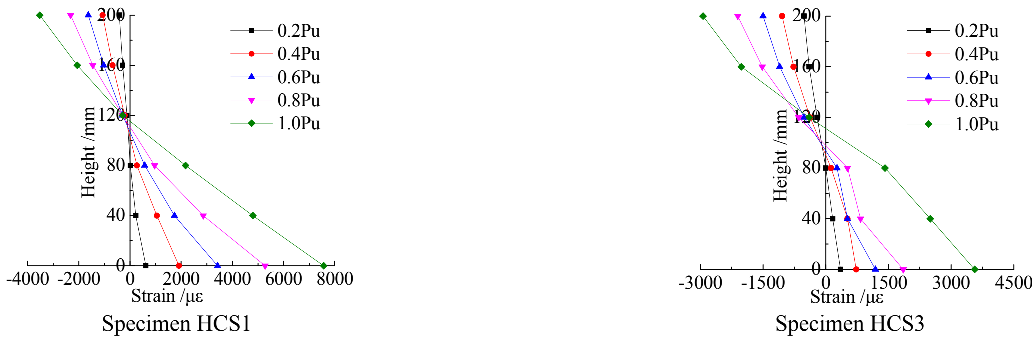

(a) Strain distribution along the section height at mid-span point

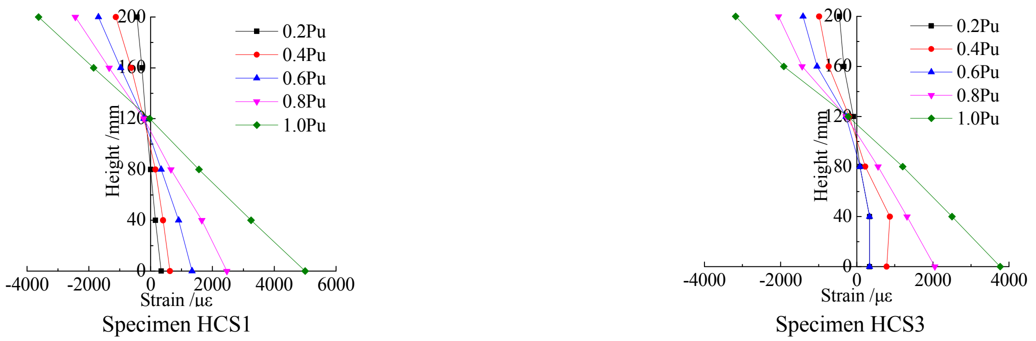

(b) Strain distribution along the section height at loading point

Fig. 8 Distribution of strain along the section height

specimen HCS3 are depicted in Fig. 7. From the load-strain curves, it can be observed that the ultimate compression strains of the top concrete are up to 3200 $\mu\varepsilon$, and the ultimate tensile strains of the bottom flat steel plate reach about 3000 $\mu\varepsilon$ to 6000 $\mu\varepsilon$ at both the mid-span point and the loading point, respectively. In other specimens, the strains of the top concrete and the steel plate are about 3000 $\mu\varepsilon$ to 4200 $\mu\varepsilon$ and 3500 $\mu\varepsilon$ to 8000 $\mu\varepsilon$, respectively. Therefore, the final failure mode of all the specimens is bending failure, with the yielding of the steel plate and the crushing of the top concrete in compression zone.

No obvious slippage was observed on the surface between the flat steel plate and the concrete for all the specimens, which indicated that the flat steel plate and the concrete performed well throughout the experiment. To verify the plane section assumption, two sets of the strain gauges were attached along the height of the section at the mid-span point and the loading point, as shown in Fig. 4. The strain distributions at these two sections in the specimen HCS1 and HCS3 are plotted in Figs. 8(a)-(b), where it can be observed that the strain distributions are in linear along the height of the section at the mid-span point and the loading point. As a result, the plane-section assumption is satisfied, and the bending capacity and the flexural rigidity of this kind of composite slab could be stablished on the basis of plane section assumption.

4. Analysis on bending capacities

Based on the experimental data and the analysis on the mechanical performance of the hollow composite slabs, the bending capacities of the specimens in both series are presented in this section.

4.1 Basic assumptions

Experimental results reported above show that the failure modes of the composite slabs in both series are the flexural failure, with the yielding of the bottom flat steel plate and the PBL shear connectors. Therefore, to obtain the bending capacity of the hollow composite slab, the following assumptions are made:

(1) The tensile strength of the concrete was neglected.
(2) The plane-section assumption was satisfied.
(3) The strength of the concrete at the compression region could reach its design compressive strength, and the resultant force of the concrete could be calculated from the equivalent rectangular stress block method.
The hollow composite slabs were ductile, and the whole cross section could be taken as in plastic stage, therefore the strength of the flat steel plate at the tension region could be taken as yield strength. The PBL shear connectors also reached the yield strength both at the compression region and at the tension region.

4.2 Bending capacity of specimens in series 1

For hollow composite slab specimens with longitudinal CHSS, the bending capacities vary with the depth of neutral axis. Therefore, to calculate the bending capacity of series 1, three positions of the neutral axis are presented as follows:

Case 1: the neutral axis is above CHSS.
When the depth of compression zone x is smaller than y_2, which means that the neutral axis is above the CHSS, and it is considered that the strength of the CHSS and the penetrated steel plate reach their yielding strength in the ultimate state. Therefore, the height x of the compression zone of concrete and the bending capacity M_{cu} of the hollow composite slabs can be calculated on the basis of the equilibrium condition of the force presented in Fig 9(a) and denoted as follows

$$x = \frac{A_d f_d + A_p f_p - A'_s f'_y}{b f_c} \le y_2 \quad (1)$$

$$\begin{aligned} M_{cu} &= A_d f_d \left(h - \frac{t_d}{2} - \frac{x}{2}\right) - A'_s f'_y \left(a'_s - \frac{x}{2}\right) \\ &+ A_p f_p \left(h - t_d - y_1 - \frac{D}{2} - \frac{x}{2}\right) \end{aligned} \quad (2)$$

Case 2: the neutral axis is within CHSS.
When the height of the compression zone of concrete x is larger than y_2 but smaller than the sum of the y_2 and the external diameter D of the CHSS, which means the neutral axis passes through the CHSS, and the part of the CHSS above the neutral axis is in compression, while the part of the CHSS below the neutral axis is in tension. The stress distribution of the whole cross section can be expressed in Fig. 9(b), where the height x of the compression zone of concrete and the bending capacity M_{cu} of the hollow composite slabs can be calculated on the basis of the equilibrium condition of the force and denoted as follows

$$y_2 < x = \frac{A_d f_d + A_{p1} f_p - A_{p2} f_p - A'_s f'_y}{b f_c} \le y_2 + D \quad (3)$$

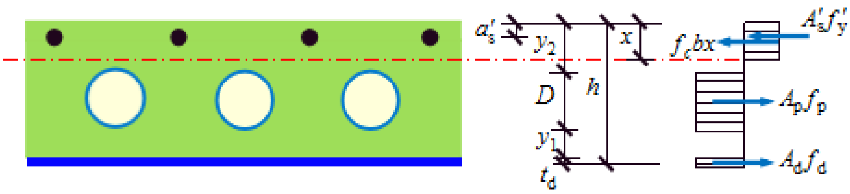

(a) The neutral axis is above the steel pipes

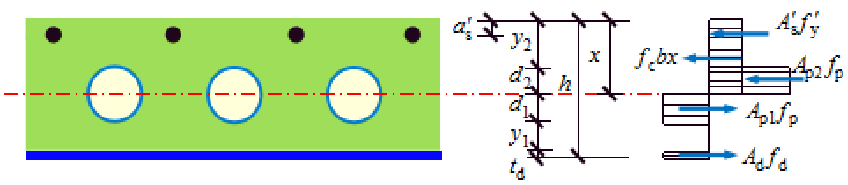

(b) The neutral axis is within the steel pipes

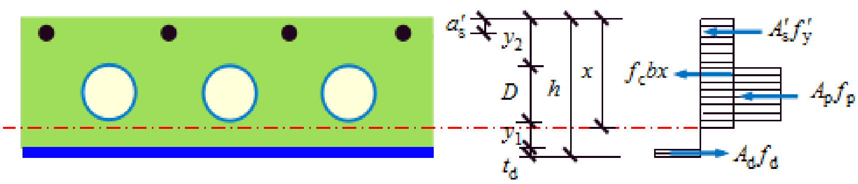

(c) The neutral axis is below the steel pipes

Fig. 9 Diagram of calculating the bending capacity for the specimens in series 1

$$M_{cu} = A_d f_d (h - \frac{t_d}{2} - \frac{x}{2}) + A_{p1} f_p (h - t_d - y_1 - \frac{d_1}{2} - \frac{x}{2})$$
$$- A_{p2} f_p (h - t_d - y_1 - d_1 - \frac{d_2}{2} - \frac{x}{2}) \quad (4)$$
$$- A'_s f'_y (a'_s - \frac{x}{2})$$

Case 3: the neutral axis is below CHSS.

When the height of the compression zone of concrete x is larger than the sum of the y_2 and the external diameter D of the steel pipe, which means the neutral axis is below the CHSS. It is considered that the CHSS is compressed to yield and the bottom flat steel plate is tensed to yield. The stress distribution of the whole cross section can be expressed in Fig. 9(c), where the height x of the compression zone of concrete and the bending capacity M_{cu} of the hollow composite slabs can be calculated on the basis of the equilibrium condition of the force and denoted as follows

$$x = \frac{A_d f_d - A_p f_p - A'_s f'_y}{b f_c} > y_2 + D \quad (5)$$

$$M_{cu} = A_d f_d (h - \frac{t_d}{2} - \frac{x}{2}) - A'_s f'_y (a'_s - \frac{x}{2})$$
$$- A_p f_p (h - t_d - y_1 - \frac{D}{2} - \frac{x}{2}) \quad (6)$$

Where, x is the height of the concrete in compression zone;

f_c is the prismatic compressive strength of the concrete;

b is the width of the hollow composite slab specimens;

h is the thickness of the slab;

D is the external diameter of the CHSS;

d is the internal diameter of the CHSS;

A_d is the cross-sectional area of the flat steel plate;

t_d is the thickness of the flat steel plate;

f_d is the yielding stress of the flat steel plate;

A_p is the cross-sectional area of the CHSS;

A_{p1} is the sectional area of the CHSS below the neutral axis, and $A_{p1} = A_p d_1/D$;

A_{p2} is the sectional area of the CHSS above the neutral axis, and $A_{p1} = A_p d_2/D$;

f_p is the yielding stress of the CHSS;

A'_S is the cross-sectional area of the upper longitudinal reinforcement;

f'_y is the yielding stress of the upper longitudinal reinforcement;

y_1 is the distance from the bottom edge of the CHSS to the top surface of the flat steel plate;

a'_S is the distance from the centroid of the longitudinal reinforcement to the top of the edge of the slab;

d_1 and d_2 are the distances from neutral axis to the bottom surface and to the top surface of the CHSS, respectively.

4.3 Bending capacity of specimens in series 2

Similar with the specimens for series 1, the bending capacities of the specimens for series 2 also vary with the depth of neutral axis. Therefore, to obtain the bending capacities of the hollow composite slabs with transverse CHSS, three positions of the neutral axis are also presented as follows:

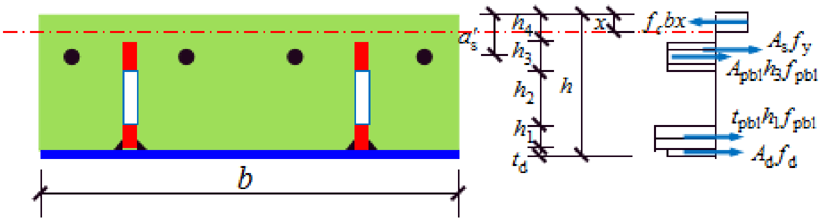

(a) The neutral axis is above the PBL plate

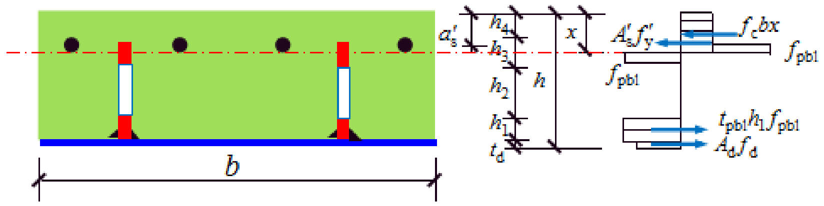

(b) The neutral axis passes through the top of the PBL plate

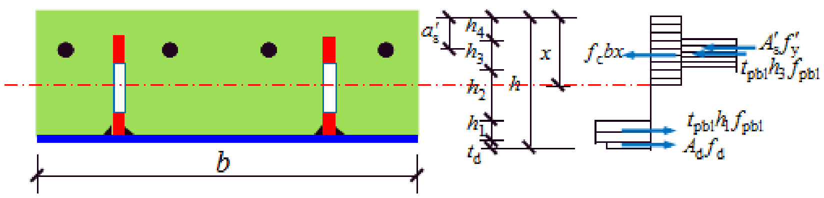

(c) The neutral axis is below the top of the PBL plate

Fig. 10 Diagram of calculating the bending capacity for the specimens in series 2

Case 1: the neutral axis is above the PBL plate.

When the height of the compression zone x is smaller than h_4, which means that the neutral axis is above the PBL plate. It is considered that the strength of the PBL plate and the bottom flat steel plate reach their yielding strength. Therefore, the height x of the compression zone and the bending capacity M_{cu} of the hollow composite slabs can be calculated on the basis of the equilibrium condition of the force presented in Fig. 10(a) and expressed as follows

$$x = \frac{A_d f_d + t_{pbl} h_1 f_{pbl} + t_{pbl} h_3 f_{pbl} + A_s f_y}{b f_c} \leq h_4 \tag{7}$$

$$\begin{aligned} M_{cu} &= A_d f_d \left(h - \frac{t_d}{2} - \frac{x}{2}\right) + t_{pbl} h_1 f_{pbl} \left(h - t_d - \frac{h_1}{2} - \frac{x}{2}\right) \\ &+ t_{pbl} h_3 f_{pbl} \left(h - t_d - h_1 - h2 - \frac{h_3}{2} - \frac{x}{2}\right) \\ &+ A_s f_y \left(a_s' - \frac{x}{2}\right) \end{aligned} \tag{8}$$

Where, t_{pbl} is the thickness of the PBL plate;

f_{pbl} is the tensile strength of the PBL plate;

h_1 is the distance from the bottom edge of the hole in PBL plate to the top surface of the flat steel plate;

h_2 is the diameter of the hole in PBL plate;

h_3 is the distance from the upper edge of the hole to the top surface of the PBL plate;

h_4 is the distance from the top surface of the PBL plate to the upper edge of the hollow composite slab.

Case 2: the neutral axis passes through the top of the PBL plate.

When the height of the compression zone x is larger than h_4 but smaller than the sum of h_3 and h_4, which means that the part of the PBL plate above the neutral axial is in compression and below the neutral axial is in tension. Because of the smaller cross-sectional areas of the PBL plate above the hole, for simplification, the contributions of this part above the hole are not taken into account in this case. It is considered that the part of PBL plate below the hole and the bottom flat steel plate are tensed to yield. Therefore, the height x of the compression zone and the bending capacity M_{cu} of the hollow composite slabs can be calculated on the basis of the equilibrium condition of the force presented in Fig. 10(b) and expressed as follows

$$x = \frac{A_d f_d + t_{pbl} h_1 f_{pbl} - A_s' f_y'}{b f_c} \leq h_3 + h_4 \tag{9}$$

$$\begin{aligned} M_{cu} &= A_d f_d \left(h - \frac{t_d}{2} - \frac{x}{2}\right) - A_s' f_y' \left(a_s' - \frac{x}{2}\right) \\ &+ t_{pbl} h_1 f_{pbl} \left(h - t_d - \frac{h_1}{2} - \frac{x}{2}\right) \end{aligned} \tag{10}$$

Case 3: the neutral axis is below the top of the penetrated plate.

When the height of the compression zone x is larger than the sum of h_3 and h_4, which means that the neutral axis passes through the hole or the part of the PBL plate below the hole. It is considered that the PBL plate above the hole is compressed to yield and the PBL plate below the hole is tensed to yield. Therefore, the height x of the compression zone and the bending capacity M_{cu} of the hollow composite slabs can be calculated on the basis of the equilibrium condition of the force presented in Fig 10(c) and expressed as follows

$$x = \frac{A_d f_d + t_{pbl} h_1 f_{pbl} - t_{pbl} h_3 f_{pbl} - A_s' f_y'}{b f_c} > h_3 + h_4 \tag{11}$$

$$\begin{aligned} M_{cu} &= A_d f_d \left(h - \frac{t_d}{2} - \frac{x}{2}\right) + t_{pbl} h_1 f_{pbl} \left(h - t_d - \frac{h_1}{2} - \frac{x}{2}\right) \\ &- t_{pbl} h_3 f_{pbl} \left(h - t_d - h_1 - \frac{h_2}{2} - \frac{x}{2}\right) \\ &- A_s f_y \left(a_s' - \frac{x}{2}\right) \end{aligned} \tag{12}$$

4.4 Verification

Based on the previous discussion, the calculated bending capacities M_{cu} for both series of hollow composite slabs are tabulated in Table 3. The calculated bending capacity for specimens with longitudinal CHSS is 134.25 kN·m, which is close to the average test results of the two specimens 147.25 kN·m. In addition, the calculated bending capacity for specimens with transverse CHSS is 114.8 kN·m, which is also close to the average test results of the three specimens 126.7 kN·m. Therefore, the bending capacity of this kind of hollow composite slabs can be reasonably predicted by proposed method.

5. Analysis on flexural rigidity

5.1 Flexural rigidity of specimens in series 1

For specimens with longitudinal CHSS, some assumptions are adopted to calculate the flexural rigidity of this kind of hollow composite slabs:

(1) The composite section of the bottom flat steel plate and the concrete slab were equivalent to the I-shaped section, as shown in Fig. 11, and the flexural rigidity of the equivalent I-shaped section could be calculated by the method for predicting the flexural rigidity of reinforced concrete member.
(2) The flexural rigidity of the composite slab was the sum of the rigidity of the equivalent I-shaped section and that of the CHSS.
(3) Therefore, the flexural rigidity of the composite slab with longitudinal steel plate could be determined with the formula (13)

$$B_s = \frac{E_s A_p h_0^2}{1.15\psi + 0.2 + \dfrac{6\alpha_E \rho}{1 + 3.5\gamma_f'}} + E_p I_p \tag{13}$$

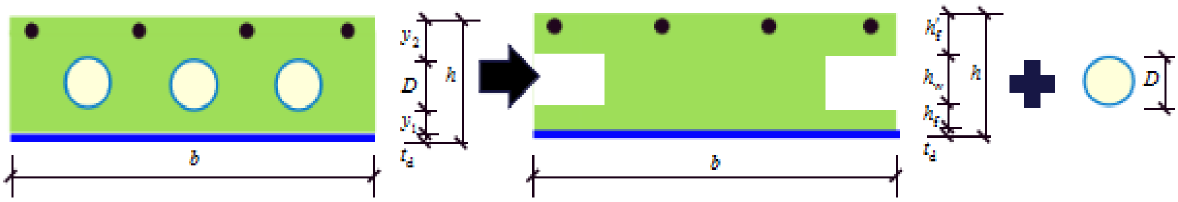

Fig. 11 Diagram of calculating the flexural rigidity for the specimens in series 1

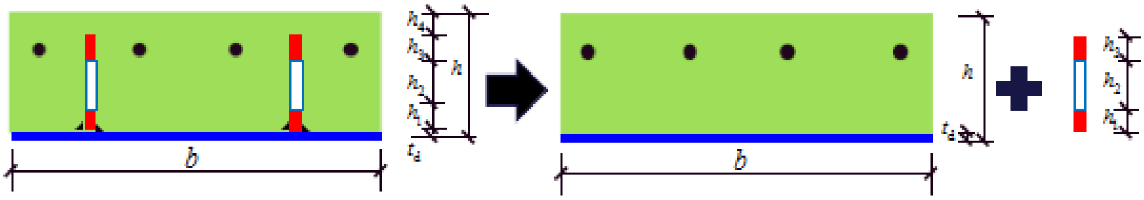

Fig. 12 Diagram of calculating the flexural rigidity for the specimens in series 2

Where, E_s and E_p are the elastic modulus of the bottom steel plate and the CHSS respectively;

I_p is the moment of inertial of the CHSS, and $I_p = \dfrac{\pi(D^4 - d^4)}{64}$;

h_0 is the effective depth of the section, and $h_0 = h - t_d/2$;

ψ is the strain inhomogeneity coefficient of bottom steel plate between cracks, and $\psi = 1.1 - 0.65\dfrac{f_{tk}}{\rho_{te}\sigma_{sk}}$, in which, ρ_{te} is the steel plate ratio at the tension zone, and $\rho_{te} = \dfrac{A_p}{A_{te}}$, A_{te} is the cross-sectional area of the effective tensile concrete, and $A_{te} = b_w h + (b - b_w)(y_1 + t_d)$, σ_{sk} is the stress of steel plate under normal work condition, $\sigma_{sk} = \dfrac{M_{sk}}{0.87 h_0 A_p}$, M_{sk} is the largest bending moment of the specimen under normal work condition;

α_E is the ratio of the elastic modulus of the steel plate to that of the concrete, and $\sigma_E = \dfrac{E_s}{E_c}$;

ρ is the steel plate ratio of the whole cross section, and $\rho = \dfrac{A_p}{b_w h_0}$;

γ'_f is the area of the flange at compression to that of the web, and $\gamma'_f = \dfrac{(b - b_w) y_2}{b_w h_0}$; and other variables are defined as before.

5.2 Flexural rigidity of specimens in series 2

Same assumptions as series 1 specimens were made, but it should be point out that the flexural rigidity of the composite slab with transverse CHSS was the sum of the rigidity of the equivalent I-shaped section and that of PBL plate instead of that of the CHSS, the calculation diagram is shown in Fig. 12. Therefore, the flexural rigidity of the specimens with transverse CHSS could be determined as follow

$$B_s = \frac{E_s A_p h_0^2}{1.15\psi + 0.2 + 6\alpha_E \rho} + E_{pbl} I_{pbl} \tag{14}$$

Where, E_{pbl} and I_{pbl} are the elastic modulus and the moment of inertial of the PBL plate, respectively. A_{te} = $0.5bh$, and other variables are the same as before.

Table 4 comparison of the test value and the calculated value with formulas (13) and (14)

Series No.	Specimen No.	40%P_u			50%P_u			60%P_u		
		Δ_c	Δ_e	Δ_c/Δ_e	Δ_c	Δ_e	Δ_c/Δ_e	Δ_c	Δ_e	Δ_c/Δ_e
1	HCS1	8.06	7.70	1.047	10.15	9.90	1.025	12.34	12.40	0.995
	HCS2	8.33	8.50	0.980	10.36	10.70	0.968	12.47	13.20	0.945
Average value				1.014			0.997			0.970
2	HCS3	6.55	6.90	0.949	8.28	8.80	0.941	10.00	10.70	0.935
	HCS4	6.05	6.60	0.917	7.73	8.60	0.899	9.34	10.80	0.865
	HCS5	5.85	6.20	0.944	7.25	7.80	0.929	8.82	9.80	0.900
Average value				0.936			0.923			0.900

*Note: P_u denotes the ultimate load, Δ_c denotes the calculated value and Δ_e denotes the test value

5.3 Validation

Based on the proposed method above, the flexural rigidities of the specimens under different load levels are calculated and listed in Table 4, where P_u represents the ultimate load of each specimen. From Table 4, it can be observed that the flexural rigidity of such hollow composite slabs can be reasonably estimated by the proposed Eqs. (13)-(14). However, compared with the calculated results of series 2, the calculated results of series 1 are closer to the measured deflection, which is because the effect of the shear deformation of specimens in series 2 has not been considered in this paper. Therefore, for hollow composite slabs with transverse CHSS, it is suggested that the deflections determined by Eq. (14) should be enlarged with an amplification coefficient of 1.10 in practical engineering application for safety.

6. Conclusions

Five specimens of an innovative kind of composite slabs were conducted and tested under static load, and the mechanical performances of this kind of composite slab were investigated. Based on the experimental results and the theoretical analyses, the following conclusions can be drawn as follows:

- In the experiment, all of the specimens in two series failed in bending failure. In addition, the bending performance in terms of bending capacity and the flexural rigidity of composite slab specimen with transverse CHSS was similar to that of the specimen with longitudinal CHSS, which indicated that the arrangement of CHSS, whether in the longitudinal direction or transverse direction, had little effect on the bending performance of this type of hollow composite slab.
- No obvious slippage observed between the bottom flat steel plate and the concrete, which indicated that all of the specimens were fully composite via the PBL plate and the stud shear connectors. The plane cross-section assumption was successfully verified by the strain distribution of the cross section in mid-span of the specimen.
- A set of methods for predicting the bending capacity of the hollow composite slabs were proposed on the basis of the plane cross-section assumption. In this method, the formulas considering three different positions of the natural axis were established for each series of specimens, and the bending capacities of five specimens were calculated, which were agreed well with the test results.
- The calculation method for evaluating the flexural rigidity of the hollow composite slab was also established. In this method, the section of the composite slab was equivalent to a special reinforced concrete section. The calculated results determined by proposed method were compared with the test results and were verified to be valid.

Acknowledgments

The experiments were sponsored by the National Research and Development Program of China (Program No.2016YFC0701400), the National Natural Science Foundation of China (Program No.50708040 and No.51778525) and also supported by the Program for Changjiang Scholars as well as the Program for Innovative Research Team of Xi'an University of Architecture and Technology.

References

Ahn, J.H., Lee, C.G., Won, J.H. and Kim, S.H. (2010), "Shear resistance of the perfobond-rib shear connector depending on concrete strength and rib arrangement", *J. Constr. Steel Res.*, **66**(10), 1295-1307.

Al-Darzi, S.Y.K., Chen, A.R. and Liu, Y.Q. (2007), "Finite element simulation and parametric studies of perfobond rib connector", *Am. J. Appl. Sci.*, **4**(3), 122-127.

Al-Deen, S., Ranzi, G. and Vrcelj, Z. (2011), "Full-scale long-term experiments of simply supported composite beams with solid slabs", *J. Constr. Steel Res.*, **67**(3), 308-321.

Altoubat, S., Ousmane, H. and Barakat, S. (2015), "Effect of fibers and welded-wire reinforcements on the diaphragm behavior of composite deck slabs", *Steel Compos. Struct., Int. J.*, **19**(1), 153-171.

Ekmekyapar, T., Al-Eliwi, B.J.M., Faraj, R.H., Göğüş, M.T. and Al-Shaar, A.A.M. (2017), "Performance of lightweight aggregate and self compacted concrete filled steel tube columns", *Steel Compos. Struct., Int. J.*, **25**(3), 299-314.

Ferrer, M., Marimon, F. and Casafont, M. (2018), "An experimental investigation of a new perfect bond technology for composite slabs", *Constr. Build. Mater.*, **166**, 618-633.

GB/T 700-2006 (2006), Carbon structure steels; China Planning Press, Beijing, China.

Jiang, J., Main, J.A., Weigand, J.M. and Sadek, F.H. (2018), "Thermal performance of composite slabs with profiled steel decking exposed to fire effects", *Fire Safety J.*, **95**, 25-41.

Johnson, R.P. (2008), *Prediction of Shear Resistance of Headed Studs in Troughs of Profiled Sheeting*, Blackwell Pub.

Kataoka, M.N., Friedrich, J.T. and Debs, A.L.H.C.E. (2017), "Experimental investigation of longitudinal shear behavior for composite floor slab", *Steel Compos. Struct., Int. J.*, **23**(3), 351-362.

Leon, R.T., Perea, T, Rassati, G.A. and Lange, J. (2008), "Composite Construction in Steel and Concrete VI", *Proceeding of the 2008 Composite Construction in Steel and Concrete Conference*, Tabernash, CO, USA, July.

Mirza, O., Kaewunruen, S., Kwok, K. and Griffin, D.W.P. (2016), "Design and modelling of pre-cast steel-concrete composites for resilient railway track slabs", *Steel Compos. Struct., Int. J.*, **22**(3), 537-565.

Oehlers, D. and Bradford, M. (1995), *Composite Steel and Concrete Structural Members: Fundamental Behaviour*, Elsevier Science, Pergamon, Oxford, England.

Oguejiofor, E.C. and Hosain, M.U. (1994), "A parametric study of perfobond rib shear connectors", *Can. J. Civil Eng.*, **21**(4), 614-625.

Qiao, W.T., An, Q., Wang, D. and Zhao, M.S. (2016), "Study on mechanical behaviors of cable-supported ribbed beam composite slab structure during construction phase", *Steel Compos. Struct., Int. J.*, **21**(1), 177-194.

Siekierski, W. (2016), "Analysis of concrete shrinkage along truss bridge with steel-concrete composite deck", *Steel Compos.*

Struct., Int. J., **20**(6), 1237-1257.

Su, Q., Yang, G. and Bradford, M.A. (2016), "Bearing capacity of perfobond rib shear connectors in composite girder bridges", *J. Bridge Eng.*, **21**(4), 06015009.

Tang, C.W. (2017), "Uniaxial bond stress-slip behavior of reinforcing bars embedded in lightweight aggregate concrete", *Struct. Eng. Mech., Int. J.*, **62**(5), 651-661.

Uy, B. and Bradford, M.A. (1996), "Elastic local buckling of steel plates in composite steel-concrete members", *Eng. Struct.*, **18**(3), 193-200.

Vianna, J.D.C., Andrade, S.A.L.D., Vellasco, P.C.G.D.S. and Costa-Neves, L.F. (2013), "Experimental study of perfobond shear connectors in composite construction", *J. Constr. Steel Res.*, **81**(81), 62-75.

Wei, X., Xiao, L. and Pei, S. (2015), "Shear behavior of multi-hole perfobond connectors in steel-concrete structure", *Struct. Eng. Mech., Int. J.*, **56**(6), 983-1001.

Yang, Y., Yu, Y., Zhou, X., Roeder, C.W. and Huo, X. (2016), "Study on mechanical performance of composite beam with innovative composite slabs", *Steel Compos. Struct., Int. J.*, **21**(3), 537-551.

Zhang, Y.K., Han, Y.X. and Song, Z.Z. (2012), "Experimental Study on Bond Behavior of Profiled Steel Sheet-Lightweight Aggregate Concrete Composite Slab", *Adv. Mater. Res.*, **594-597**, 721-724.

Zheng, S., Liu, Y., Yoda, T. and Lin, W. (2016), "Shear behavior and analytical model of perfobond connectors", *Steel Compos. Struct., Int. J.*, **20**(1), 71-89.

BU